

NRC Publications Archive Archives des publications du CNRC

Hall sensor notch detection in a through-transmission eddy current arrangement

Dionne, Leo; Mandache, Caitlin; Perron, Joel; MacMillan, John

For the publisher's version, please access the DOI link below./ Pour consulter la version de l'éditeur, utilisez le lien DOI ci-dessous.

Publisher's version / Version de l'éditeur:

<https://doi.org/10.4224/40003930>

Laboratory Technical Report (National Research Council of Canada. Aerospace. Structures, Materials and Manufacturing Laboratory); no. LTR-SMM-2025-0150, 2025-10-31

NRC Publications Archive Record / Notice des Archives des publications du CNRC :

<https://nrc-publications.canada.ca/eng/view/object/?id=b9714f61-4c20-45a5-9b2a-09e6c615975c>

<https://publications-cnrc.canada.ca/fra/voir/objet/?id=b9714f61-4c20-45a5-9b2a-09e6c615975c>

Access and use of this website and the material on it are subject to the Terms and Conditions set forth at

<https://nrc-publications.canada.ca/eng/copyright>

READ THESE TERMS AND CONDITIONS CAREFULLY BEFORE USING THIS WEBSITE.

L'accès à ce site Web et l'utilisation de son contenu sont assujettis aux conditions présentées dans le site

<https://publications-cnrc.canada.ca/fra/droits>

LISEZ CES CONDITIONS ATTENTIVEMENT AVANT D'UTILISER CE SITE WEB.

Questions? Contact the NRC Publications Archive team at

PublicationsArchive-ArchivesPublications@nrc-cnrc.gc.ca. If you wish to email the authors directly, please see the first page of the publication for their contact information.

Vous avez des questions? Nous pouvons vous aider. Pour communiquer directement avec un auteur, consultez la première page de la revue dans laquelle son article a été publié afin de trouver ses coordonnées. Si vous n'arrivez pas à les repérer, communiquez avec nous à PublicationsArchive-ArchivesPublications@nrc-cnrc.gc.ca.

Hall Sensor Notch Detection in a Through-Transmission Eddy Current Arrangement

Classification: Non-sensitive
Distribution: Unlimited
Report No.: LTR-SMM-2025-0150
Date: October 31st, 2025
Author(s): Leo Dionne, Catalin Mandache, Joel Perron, John MacMillan



Executive Summary

Detection of non-surface fatigue cracking represents a challenge for most conventional non-destructive inspection (NDI) techniques. This report discusses a custom electromagnetic solution and demonstrates its capabilities and shortcomings. The laboratory experiments used aluminium plates with fastener holes and notches. The notch length and penetration depth varied from 1 to 6 mm and from 25 to 100% through-wall thickness, respectively.

This work embodies a two-fold novelty: (i) the through-transmission eddy current approach, with a stationary driving coil, attached to the far-side of the specimen, and (ii) the use of Hall effect solid-state sensors for the detection of the magnetic field generated by the eddy current flow in an aluminium plate containing crack-like discontinuities.

The experimental results confirm that the notch characteristics, particularly the depth and length, significantly affect the magnetic response as sensed by the Hall-effect probe. The field amplitude increased with the notch length, as well as with its degree of penetration through the wall of the aluminium plate. A direct correlation between the notch length and the signal strength was established; however, for notches penetrating less than 75% of the wall thickness, no useful signal was detected. This outcome was assumed to be due to the shielding effect of the eddy currents flowing in the conductive material on top of the partially penetrating notch.

Table of contents

Executive Summary	iii
Table of contents	iv
List of Figures.....	v
List of Tables	vi
List of Abbreviations	vii
1 Introduction	1
1.1 Background.....	1
1.2 Scope.....	1
1.3 Objectives	1
2 Methods	2
2.1 Spiral coil characteristics.....	2
2.2 Hall-effect sensor	3
2.3 Hall sensor calibration.....	5
2.4 Experimental setup	7
3 Results	12
4 Discussion.....	17
5 Conclusion	19
6 References.....	20
Appendix A: Surface scans representation.....	A-1
Appendix B: MATLAB code examples	B-1
B.1 Display C-scan and profile	B-2
B.2 Apply circular filter and rotation.....	B-5
B.3 Identify the centre of the fastener hole	B-6

List of Figures

Figure 1: Photograph of the planar spiral coil.....	2
Figure 2: Schematic of a Hall-effect sensor [3].....	4
Figure 3: The SS484B Hall-effect sensor by Honeywell: (a) photograph, (b) dimensions and pin schematic [4]	5
Figure 4: Photographs of the Helmholtz coils pair used for the calibration of the Hall sensor	5
Figure 5: Sensitivity of the Hall sensor with the magnetic field – DC configuration	6
Figure 6: Sensitivity of the Hall sensor with the magnetic field – AC configuration.....	7
Figure 7: Photograph of the spiral planar coils attached to the specimen and connected in series.....	8
Figure 8: Schematic representation of the experimental setup (features of the part are not to scale).....	8
Figure 9: Schematic view of the back side of the specimen showing the three partially penetrating notches and the through-wall notch (right)	9
Figure 10: Honeywell SS494B Hal sensor in its custom holder.....	9
Figure 11: Hall sensor C-scans of the spiral PCB coil: the generated magnetic field at various frequencies	10
Figure 12: Hall sensor scans of 6 mm notches: left – through-notch, right – 75% penetration notch from the far side.....	11
Figure 13: Processed experimental data looking at various notch lengths and penetration depths.....	13
Figure 14: Directions of parallel and perpendicular to notch profiles in a C-scan.....	14
Figure 15: Profiles for the 6 mm notch: parallel (left) and perpendicular (right) to the notch, 100% and 75% notch depth cases	14
Figure 16: Profiles for the 4 mm notch: parallel (left) and perpendicular (right) to the notch, 100% and 75% notch depth cases	15
Figure 17: Profiles for the 2 mm notch: parallel (left) and perpendicular (right) to the notch, 100% and 75% notch depth cases	15
Figure 18: Profiles for the 1 mm notch: parallel (left) and perpendicular (right) to the notch, 100% and 75% notch depth cases	15
Figure 19: Maximum magnetic field along a profile scan parallel to the through-wall notch	16
Figure 20: Differences in eddy current flow for a through-wall crack (left) and a partially penetrating one (right).....	18

List of Tables

Table 1: Geometrical characteristics of the spiral coils. 2

List of Abbreviations

AA	Aluminium Alloy
AC	Alternating Current
DC	Direct Current
EDM	Electrical Discharge Machining
NDE	Non-Destructive Evaluation
NDI	Non-Destructive Inspection
NDT	Non-Destructive Testing
PCB	Printed Circuit Board

1 Introduction

Aircraft structures contain critical components that are difficult to physically reach for inspection and maintenance. Their complex geometry and location make inspection without disassembly extremely difficult. Moreover, for eddy current testing the inspection is further restricted due to the limited skin depth of penetration. This report proposes an avenue to alleviate this challenge: using a through-transmission technique with an embedded, printed circuit board (PCB) eddy current coil for excitation and a Hall effect solid-state device for sensing.

1.1 Background

Eddy current is one of the main techniques of non-destructive testing (NDT), with preponderant use in aerospace and nuclear industries. Eddy currents are generated in electrically conductive materials by a time varying magnetic flux, according to Faraday's law of induction. As the current flow follows the path of least resistance in the tested part, it can be used to indicate localized discontinuities, such as fatigue cracks in multi-layer aluminium alloy aircraft structures. However, being a diffusion process, the eddy current technique suffers from a limited depth of penetration, especially when the excitation and sensing are performed from the same side of a part.

This work proposes the use of thin, flexible, printed-circuit spiral coils as in-situ drivers of eddy current, placed at the far side or within a multi-layer structure, while the sensing is performed with magnetic field sensitive solid-state devices, such as Hall sensors. This type of arrangement is especially suited for structures where disassembly is not desired, as due to time constraints or the risk of introducing additional damages. The excitation PCB coils could be attached to the aerospace structure under investigation at the time of manufacture or during the overhaul. These flexible coils are compact, electrically insulated, light-weight, and cost-effective.

1.2 Scope

The report investigates a through-transmission eddy current arrangement, with the PCB coil attached to the far side of an aluminium specimen containing electrically discharge machined (EDM) notches, while a Hall sensor scans the top surface of the specimen with the goal of detecting the magnetic flux discontinuities introduced by the notches. The EDM notches are rectangular in shape and oriented radially, in the same direction, from fastener holes. They could partially or fully penetrate the thickness of the aluminium coupon.

1.3 Objectives

The eddy current technique has challenges in detecting non-surface open discontinuities due to its intrinsic depth of penetration limitations. To alleviate these shortcomings, the objective of this work is to assess the feasibility of using Hall sensors to detect artificially introduced flaws, *i.e.* notches, of different length and wall-penetration (from the far-side of the part).

2 Methods

2.1 Spiral coil characteristics

Flexible substrates were used as a base for fabrication of planar, surface-conformable spiral coils, as used for the excitation in this work. Figure 1 shows an example of such coil.



Figure 1: Photograph of the planar spiral coil

The geometrical specifications of this stationary coils are given in Table 1.

Table 1: Geometrical characteristics of the spiral coils.

Number of turns	n	14
Inner diameter (mm)	d_{in}	7
Outer diameter (mm)	d_{out}	21
Trace width (μm)	w	300
Spacing (μm)	s	300

The inductance of the coil, L , is given by the following equation [1, 2]:

$$L = \frac{\mu \cdot n^2 \cdot d_{avg}}{2} \cdot \left(\ln \left(\frac{2.46}{\rho} \right) + 0.2 \cdot \rho^2 \right) \quad (1)$$

With μ being the permeability of the core (in this case, air), and with the average diameter, d_{avg} , and fill factor, ρ , given by equations (2) and (3), respectively:

$$d_{avg} = \frac{d_{in} + d_{out}}{2} \quad (2)$$

$$\rho = \frac{d_{out} - d_{in}}{d_{out} + d_{in}} \quad (3)$$

These relationships indicate the self-inductance of the coil to be 2.83 μH . However, the coil generates a magnetic field that induces eddy currents in a nearby conducting part, and a secondary, opposing field in the material being observed, that counteract the incident, driving magnetic field. As a result, not all the magnetic field generated by the coil on one side of the specimen will reach the other, if any. Most of the field will be attenuated, or diffused by the conductive material, but this depends on the electrical conductivity, σ , magnetic permeability, μ , as well as the driving frequency, f , as given by the skin dept equation, δ . This is the depth in the materials at which the incident magnetic field decreases by a factor equal to $1/e$ or 37% of its value at the surface.

$$\delta = \frac{1}{\sqrt{\pi \cdot \mu \cdot \sigma \cdot f}} \quad (4)$$

Based on this relationship, only about 5% of the magnetic field amplitude at the surface of the part remains at three skin depths, $3 \times \delta$. For an aluminium alloy material (2024-T4 AA) of a thickness of 1.0 mm, an electrical conductivity of 18.5 MS/m, and a testing frequency of 10 kHz, the skin depth of penetration is 1.1 mm. The choice of frequency is not only to allow the magnetic field to investigate the whole thickness of the part, but also to operate within the optimal frequency range of the Hall effect magnetic field sensor, as discussed in the following sections.

2.2 Hall-effect sensor

Hall sensors are extensively used as magnetic field readers for the magnetic flux leakage non-destructive evaluation (NDE) applications, but are not commonly applied for eddy currents techniques. They are effective in detecting discontinuities in the properties of ferromagnetic materials.

The Hall effect was discovered in 1879, by then doctorate student Edwin Herbert Hall. Although the Hall effect exists in any conducting materials, the effect only caught up with the development of the semiconductor materials (InSb, InAs, GaAs), in the second part of the twentieth century. A Hall sensor is a four-terminal solid-state device that produces an output voltage proportional to the product of its input current, I , and the magnetic flux component that it detects, B . By holding its input current constant, the Hall sensor output is proportional to the magnetic flux. The schematic shown in Figure 2 explains the Hall effect: the charge carriers in the solid-state device move on opposite sides of the cell, under the influence of the Lorentz force.

$$\vec{F}_{Lorentz} = q(\vec{v} \times \vec{B}) \quad (5)$$

The negative and positive charges are separated by the Lorentz force, when they enter the device with a velocity \mathbf{v} in the external magnetic field \mathbf{B} .

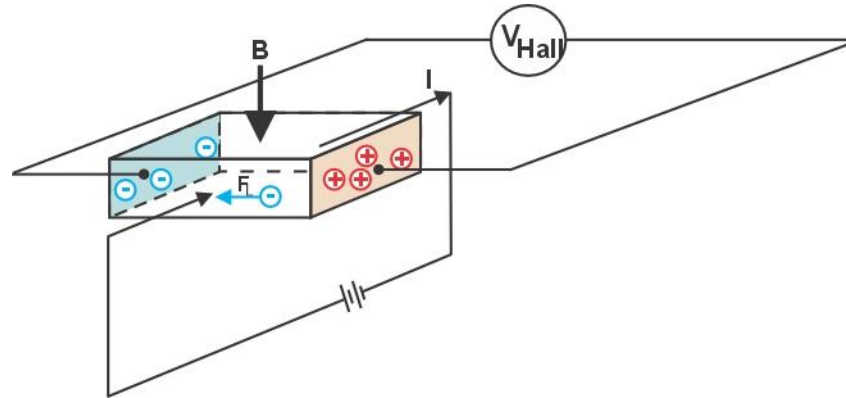


Figure 2: Schematic of a Hall-effect sensor [3]

This separation of charges introduces a potential difference, and it represents the output of a Hall-effect magnetic field sensor. The voltage is given by the following equation:

$$V_{Hall} = k_H \cdot I \cdot B \cdot \sin \theta \quad (6)$$

where θ is the angle made by the field to the input current, and k_H is the open circuit sensitivity of the sensor.

When packaged, the Hall sensor is a device with three pins, and has a set sensitivity, as well as magnetic field range. An SS494B Hall sensor, as shown in Figure 3, fabricated by Honeywell, was used in this study [4]. It has an operating temperature range between -40 and 125 °C, a required supply voltage of 5 Vdc, and a linearity range between -375 to 375 G. The typical sensitivity for this type of sensor is pf 5 mV/G. The three pins of the Hall sensor are for: input voltage, output voltage, and a common ground.

Typical applications of Hall-effect sensors are for: basic current sensing for motors, linear or angular displacement measurement, current sensing in appliances, magnetic code reading for safe and security control systems, but also for electromagnetic-based NDT, such as magnetic flux leakage and eddy current testing [3].

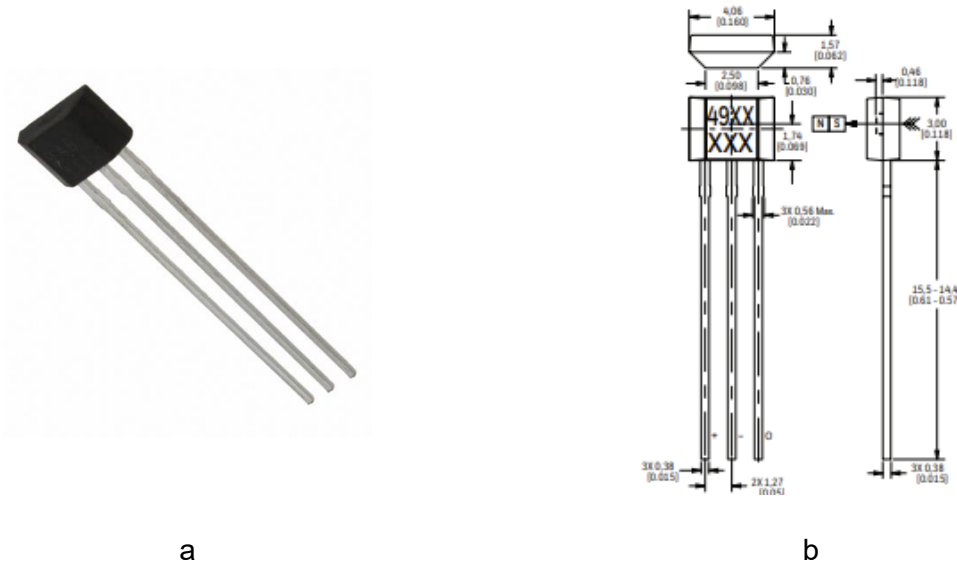


Figure 3: The SS484B Hall-effect sensor by Honeywell: (a) photograph, (b) dimensions and pin schematic [4]

2.3 Hall sensor calibration

A uniform, stable, and controllable magnetic field is necessary to determine the exact sensitivity of a Hall sensor. For this reason, a Helmholtz coil pair as shown in Figure 4 was used for calibration purposes [5, 6], with 400 turns and 15 cm median coil diameter. The magnetic field in the volume between the coil and aligned with their axis is very uniform.

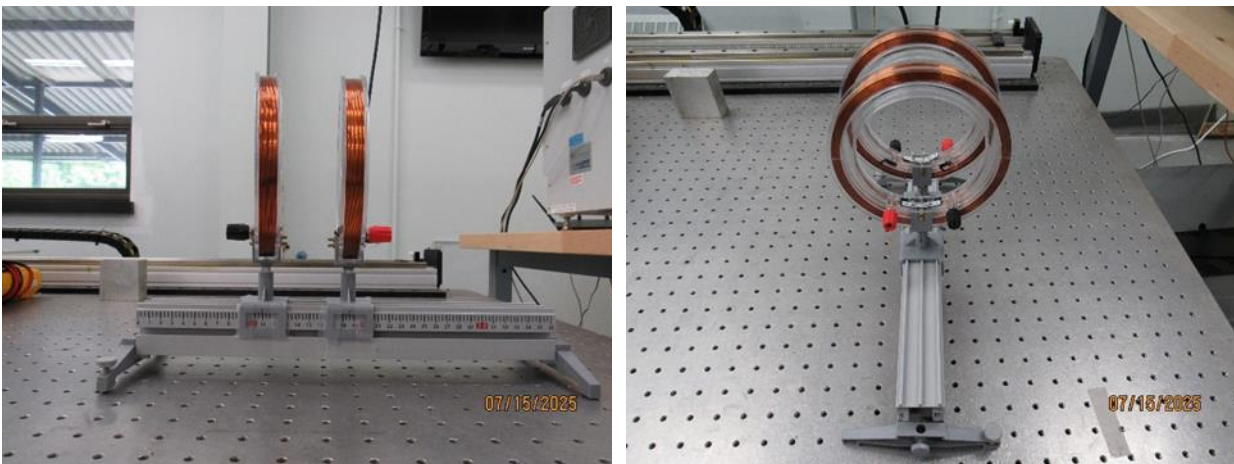


Figure 4: Photographs of the Helmholtz coils pair used for the calibration of the Hall sensor

The magnetic field created by the Helmholtz pair of coils is constant and very uniform in the middle volume between the two coils, aligned with coils' axis. The value of the magnetic field could be calculated analytically, using the following equation [5]:

$$B = \left(\frac{4}{5}\right)^{\frac{3}{2}} \cdot \frac{\mu_0 \cdot N \cdot I}{R} \quad (7)$$

Where μ_0 is the magnetic permeability of vacuum, N - the number of turns of the coil, I - the current through the coil, and R is the radius of the coil. In its most common configuration, for a uniform magnetic field in the volume between the coil pair, their centre-to-centre distance is equal to R .

With the dimensions and number of turns of the Helmholtz coils known, the magnetic field can be calculated based on equation (7) only by knowing the current flowing through the circuit. In a direct current (DC) configuration, a linear relationship is found between the Hall sensor voltage and the calculated magnetic field from varying the current through the coils, as seen in Figure 5. As determined graphically, the sensitivity of the Hall sensor is 4.65 mV/G, which is very close to the nominal value of 5 mV/G.

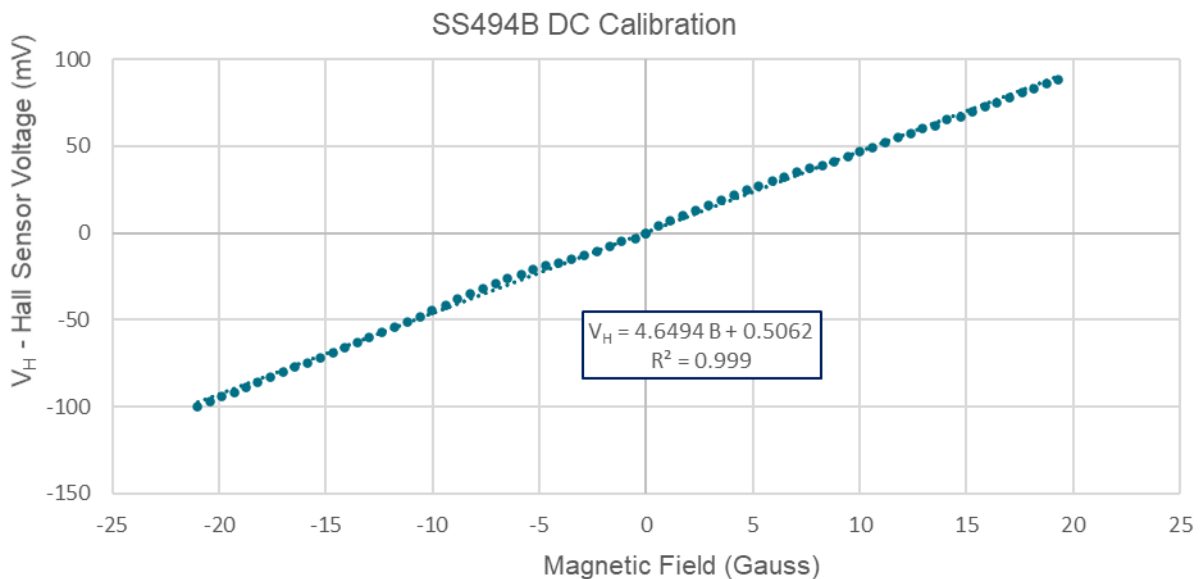


Figure 5: Sensitivity of the Hall sensor with the magnetic field – DC configuration

In an alternating current (AC) configuration a similar dependency of the Hall sensor voltage with the magnetic field was also experimentally determined, as shown in Figure 6. In this case, an alternating current of 100 Hz frequency was passed through the Helmholtz coils. In this case the sensitivity of the sensor was found to be 4.51 mV/G.

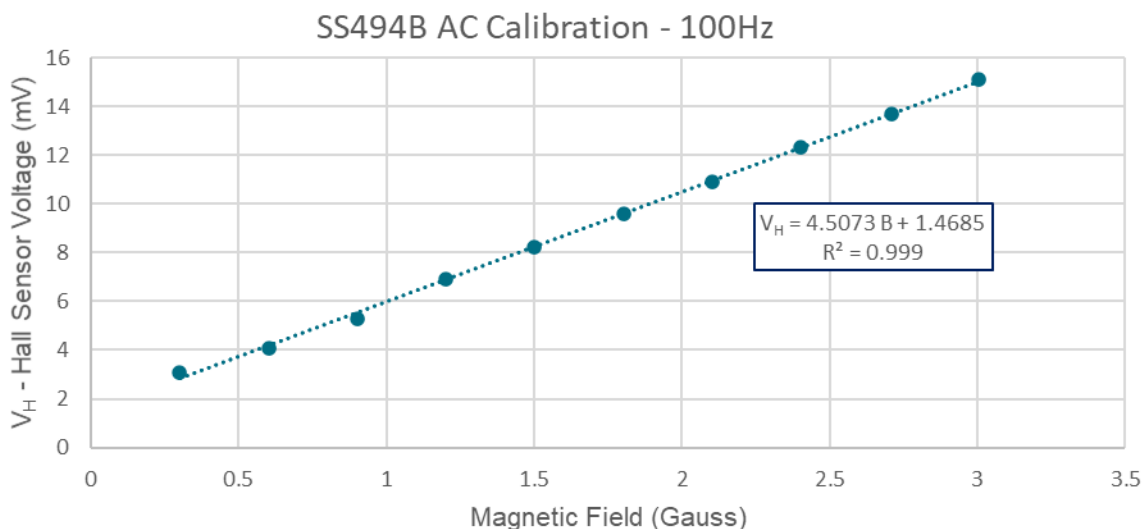


Figure 6: Sensitivity of the Hall sensor with the magnetic field – AC configuration

In the case of AC calibration, since the Helmholtz coil is an inductor, as the frequency increases, so does the impedance; therefore, it requires more voltage for maintaining the same current at higher frequencies. Due to a voltage limitation of the power source of 10 V, the maximum magnetic field that could be generated in this configuration was only 3 G, as seen in Figure 6. Although this could be regarded as a limitation, the sensitivity of the Hall sensor was determined to be very close to the one determined in the DC configuration and the nominal value of 5 mV/G, as reported in the sensor's manufacturer specifications. The differences between the DC and AC sensitivities are likely due to the nature of the inductor: in DC, the coils' reactance does not have as much of an impact on the current as in AC, where the load is mostly reactive.

2.4 Experimental setup

In this study, we investigated an aluminium plate containing fastener holes and EDM notches. The spiral coils were attached to the back side of this specimen, and centered on the fastener holes, while the top side was scanned with the SS494B Honeywell Hall-effect magnetic sensor. The TecScan eddy current scanner and the TecView2 software were used for this purpose [7]. The planar coils attached to the back of the aluminium plate were connected in series in order to pass the same current through them and, therefore, the same excitation magnetic field, as shown in Figure 7. The coils were encapsulated between polyimide layers, and were therefore electrically insulated. The magnetic field generated by the spiral coil would be counteracted by the eddy currents introduced via induction, while the scanning Hall effect sensor would record the difference between the two. A schematic of the experimental setup is shown in Figure 8. The Hall sensor is mounted in a robotic arm and is used to scan the surface of the plate.

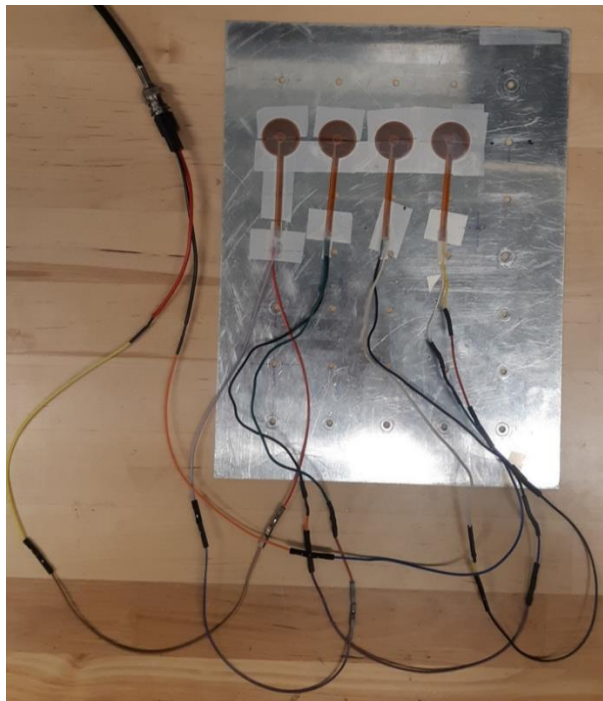


Figure 7: Photograph of the spiral planar coils attached to the specimen and connected in series

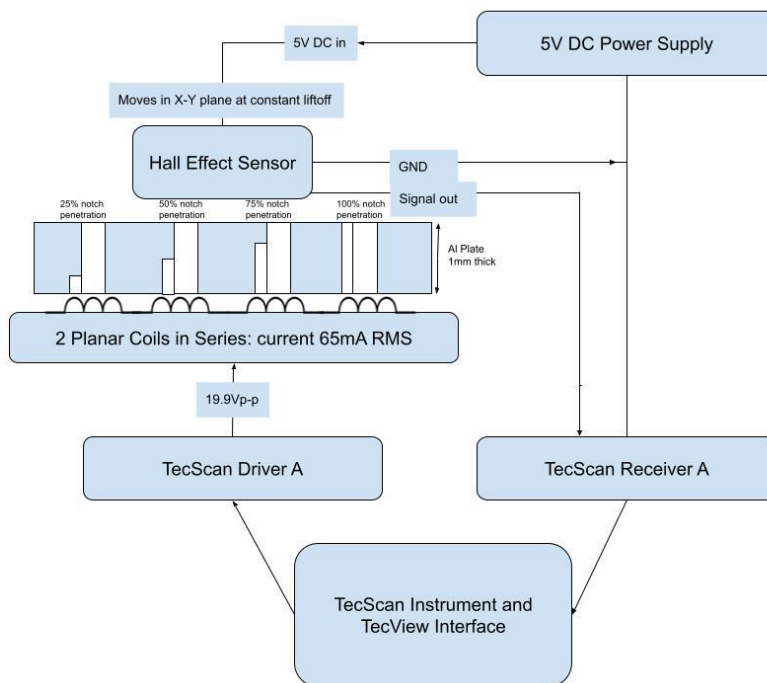


Figure 8: Schematic representation of the experimental setup (features of the part are not to scale)



Figure 9: Schematic view of the back side of the specimen showing the three partially penetrating notches and the through-wall notch (right)

The Hall sensor was powered by a 5 V DC voltage supply, while a sinusoidal waveform of 10 kHz was applied to the planar coils connected in series.

It should be noted that the output value of the scan, as presented in the TecView software is not an absolute voltage measurement, but a percentage value out of 5 V peak-to-peak, V_{pp} . For example, a data point in the C-scan that shows the value of 5, actually represents 5% of the 2.5 V amplitude ($V_{pp}/2$), meaning 125 mV. Moreover, if the signal is passed through an amplifier, say of 40 dB, meaning $100 \times$ amplification, the actual voltage output of the sensor would be 1.25 mV. When converted using the sensitivity of the Hall sensor of 5 mV/G, this represents only 0.25 G, an extremely small value, less than the background magnetic field of the Earth. The conversion is described in the Matlab analysis code included in the appendix.

To ensure consistency across measurements, a custom 3D-printed holder was manufactured based on the dimensions of the SS494B Honeywell sensor used in the experiments, as seen in Figure 10. This allowed the sensor to be levelled with the horizontal plane, *i.e.* detecting the normal-to-surface magnetic field, while the lift-off was maintained constant.



Figure 10: Honeywell SS494B Hal sensor in its custom holder

To determine the optimal frequency, a series of experimental trials was performed, with the Hall sensor scanning atop of the stationary spiral PCB coil, with no material, only air in between the two. This allowed the Hall sensor to evaluate the magnetic field produced by the coil with no other interference. Appendix A discusses how the amplitude of the receiver is found in TecView software. Figure 11 shows the amplitude results of these

scans at various frequencies. All other scanning parameters were kept the same. The driver-to-receiver, *i.e.* coil to Hall sensor distance is the same as in the case of subsequent scans with the aluminium specimen between them. From Figure 11, it could be observed not only that the signal amplitude decreases with increasing frequency but also a distortion is present, as seen in the asymmetry of the surface scans. The lower magnetic field amplitude with increasing frequency is due to the lower current flowing through the coil, as a result of higher impedance.

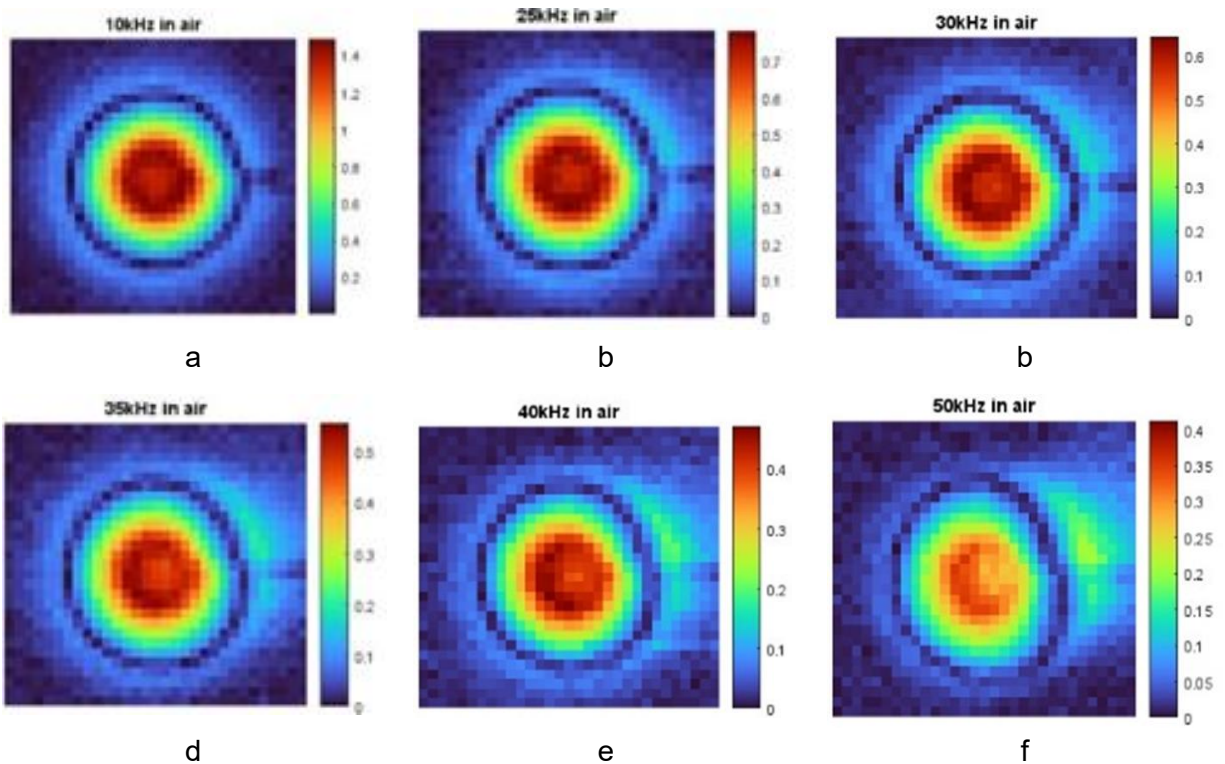


Figure 11: Hall sensor C-scans of the spiral PCB coil: the generated magnetic field at various frequencies

In the amplitude scans shown in Figure 11, the results seem almost circular – consistent with the geometry of the spiral coil, especially for frequencies of less than 30 kHz. The geometrical distortion in the scans might be due to the Hall sensor response or other scan parameters; however, in order to assure uniformity and maximum electromagnetic coupling between the driving coil and Hall sensor, a frequency of 10 kHz was chosen for all subsequent scans.

The consistent distortion on the right side of all scans is due to the connecting leads of the spiral coil. In order to avoid this unwanted interference, in the subsequent experiments, the notch direction was selected not to have the same direction as the connecting leads, and preferably, to have an opposite orientation, at 180° from the leads.

In Figure 12, a sample scan using two spiral coils connected in series; therefore, driven with the same current (that generates the same magnetic field in air), is shown for exemplification. The field produced by the flow of eddy current around the fastener holes was picked up by the Hall sensor. The Hall sensor scanned the surface above two fastener holes, with one containing a 6 mm 100% through-plate notch, while the other has a 75% through-plate penetration. The latter notch is not open to the scan surface. The differences in magnitude are substantial and the partially penetrating notch is barely visible. The portion of eddy current flowing on top of the 75% penetration notch almost completely shields the discontinuity from being detected by the Hall sensor. However, minute changes still exist and it is up to the instrumentation used to be sufficiently sensitive to detect these changes.

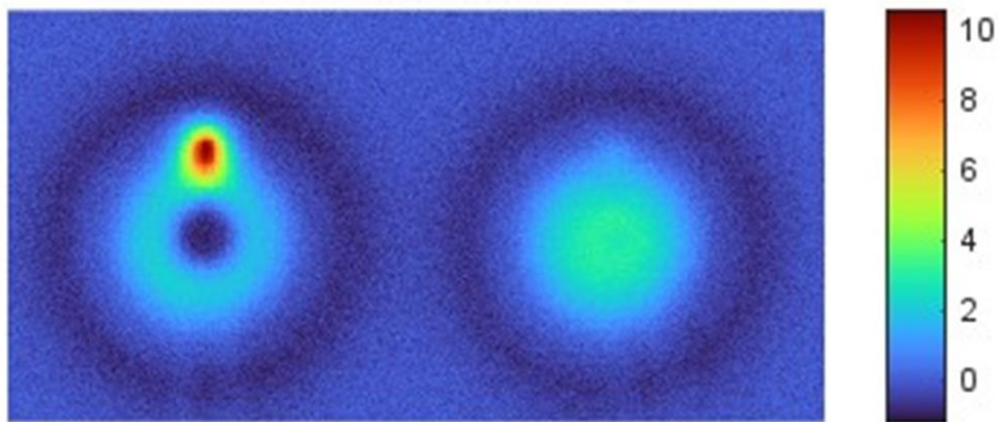


Figure 12: Hall sensor scans of 6 mm notches: left – through-notch, right – 75% penetration notch from the far side

3 Results

The data collected experimentally was post-processed using the Matlab software [8]. In a first stage, the individual pixels from the scanned image were clustered together and the points with a magnitude close to zero were removed. This was done by creating a circular filter whose size was based on a small percentage of the largest value in the amplitude, and assigning a value of zero to those data points. In the second stage, the data was centered in order to assist in the comparison of different scans. Also, lift-off compensation was performed by shifting the phase in such a way that one of the components of the impedance was aligned with the horizontal axis.

Larger notches create a larger perturbation in the eddy currents flow and the resulting magnetic field they generate; therefore, as the notch length increases, its effect on the magnetic field becomes more noticeable.

In the following figure (Figure 13), the differences between four notches, of 6-, 4-, 2-, and 1-mm lengths, and varying depths are visually compared. Only results for the largest notch size considered, 6 mm, are shown for 50% and 25% through-plate penetration. For the smaller notch lengths (4-, 2-, and 1-mm) the C-scans are not shown as these are very similar to the ones from the 6 mm notch, and the same penetration, with no indication of the notch.

A simple visual of the notch in a scan takes five centre columns or rows (depending on the desired orientation) and plots their average against position. For this representation, the data recorded in terms of percentage value could be converted into G, using the following relationship. Note that only the Y-component of the scan is taken into account, as the X-component is aligned with the lift-off variation.

$$B (G) = \frac{Y(\%) \cdot 2.5V / 100\% \cdot 10^{\left(\frac{Gain}{20}\right)}}{Sensitivity} \quad (8)$$

The 2.5 V is the maximum voltage amplitude used by the TecView software (*i.e.*, 5 V_{pp}). The gain value was maintained in most cases at 40 dB, unless otherwise specified. The denominator of equation (8) incorporates the SS494B Hall sensor sensitivity. The value specified by the manufacturer for sensitivity was 5 mV/G [4], but was found experimentally to be between 4.51 and 4.65 mV/G. Figure 14 shows a typical scan and the two orthogonal profiles extracted for further analysis: parallel to the notch and perpendicular to the notch. Since no changes were observed for the 50% and 25% notch penetrations, we did not replicate the figures, but replaced them with “X”.

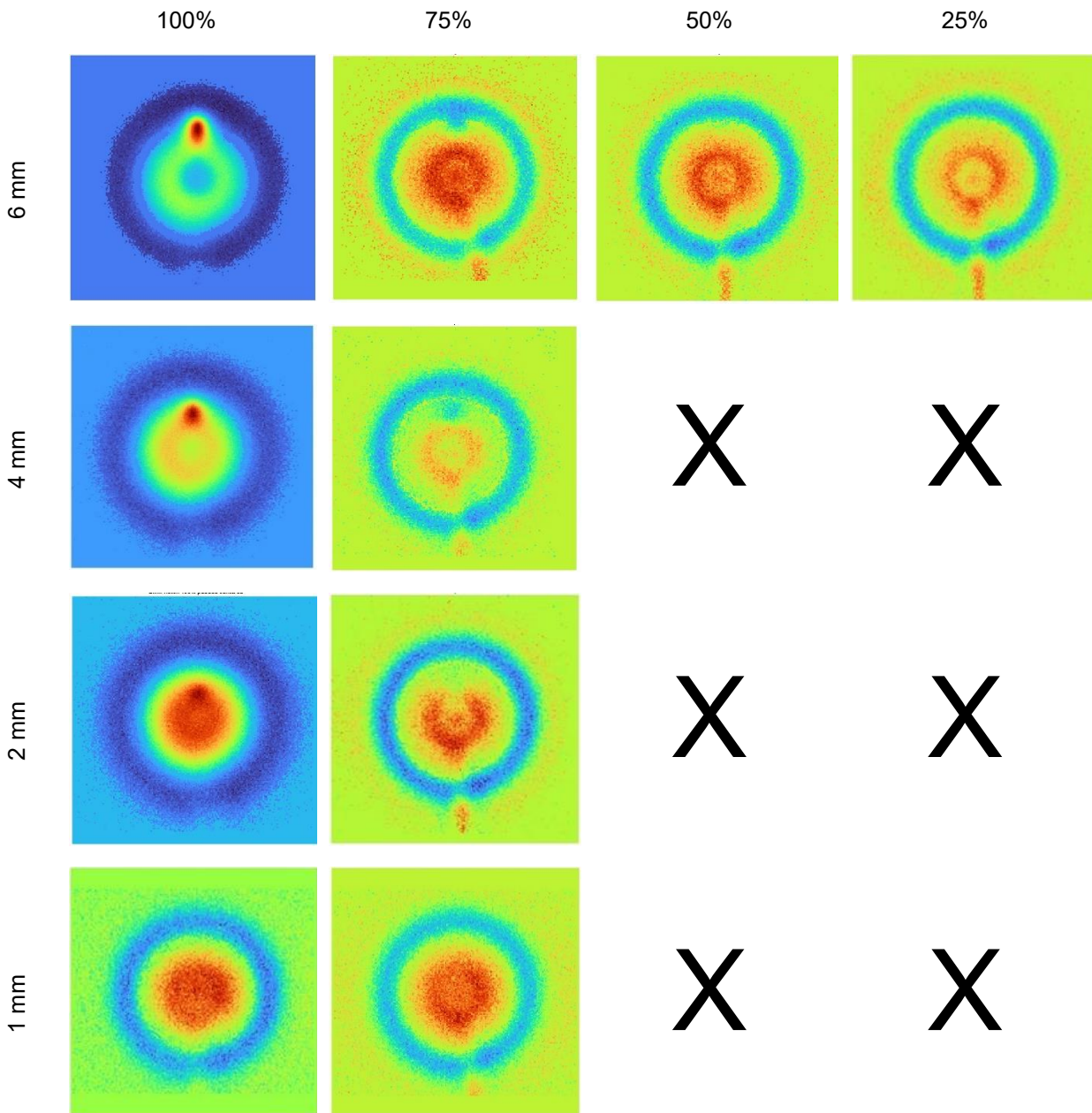


Figure 13: Processed experimental data looking at various notch lengths and penetration depths

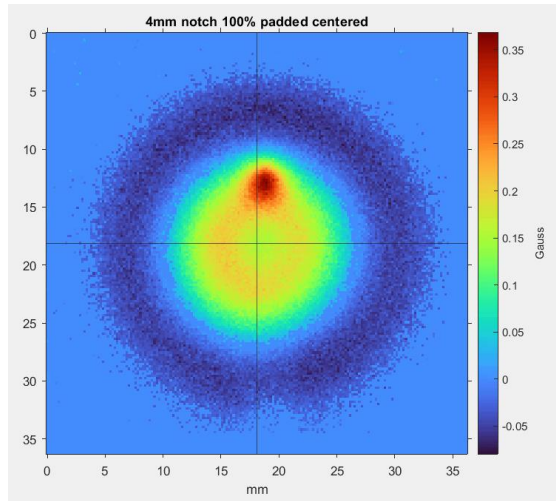


Figure 14: Directions of parallel and perpendicular to notch profiles in a C-scan

As expected, the profile along the notch (parallel or vertical profile) will have a higher degree of asymmetry, while the profile perpendicular (or horizontal) to the notch will be mostly symmetric, with any unbalance expected to be due to the non-circularity of the spiral driving coil.

The profiles for the cases depicted as C-scans in Figure 13 are shown below, in Figure 15. Despite the relatively high background noise level, it can be observed that not only are the through-notch cases consistently obvious for the 6-, 4-, and 2-mm notch lengths, but also that the peak amplitude decreases with notch length. The central line of symmetry is represented by the vertical line in each plot in Figures 15-18.

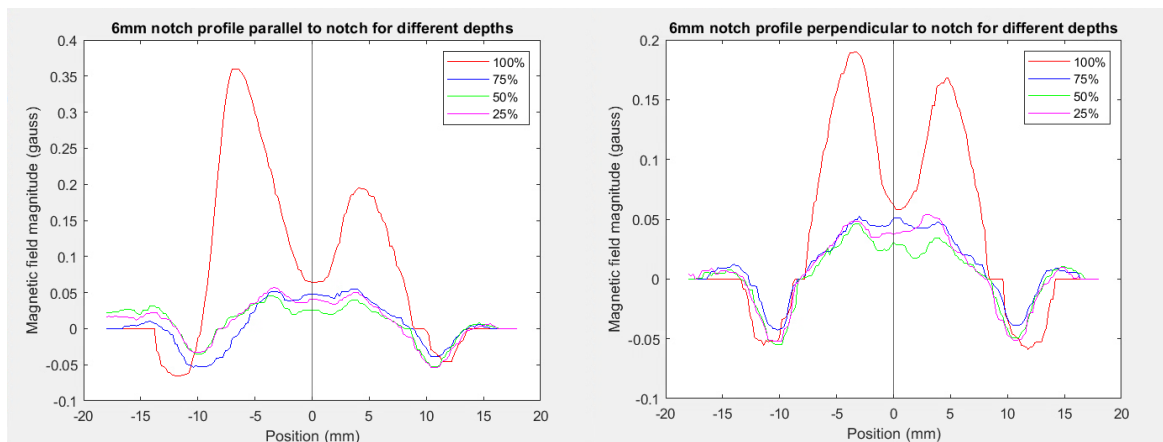


Figure 15: Profiles for the 6 mm notch: parallel (left) and perpendicular (right) to the notch, 100% and 75% notch depth cases

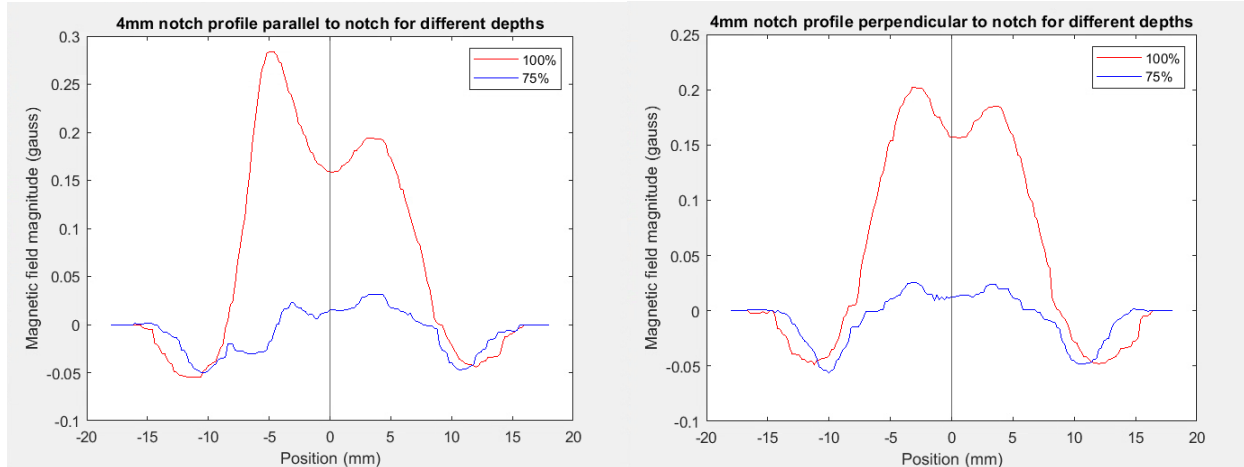


Figure 16: Profiles for the 4 mm notch: parallel (left) and perpendicular (right) to the notch, 100% and 75% notch depth cases

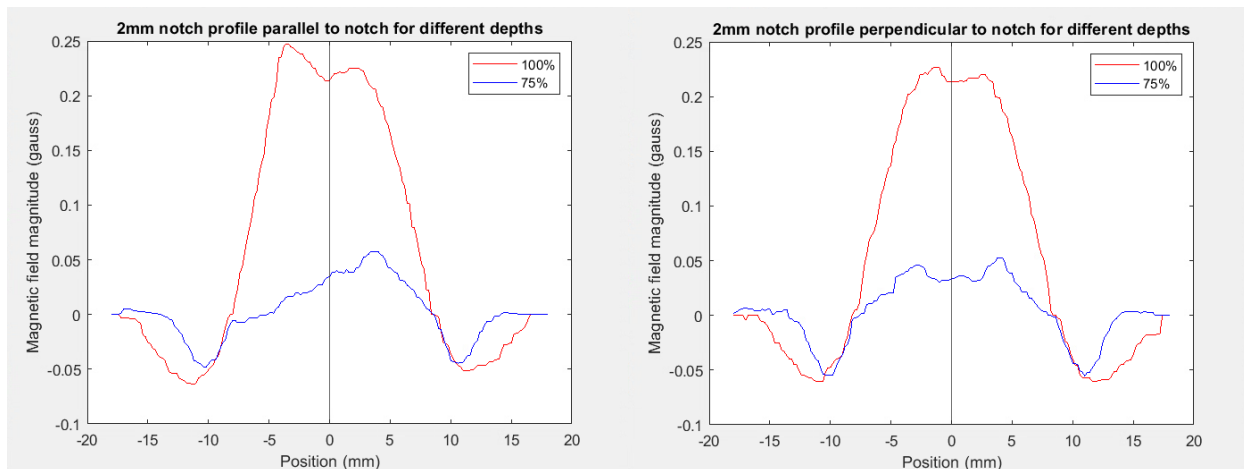


Figure 17: Profiles for the 2 mm notch: parallel (left) and perpendicular (right) to the notch, 100% and 75% notch depth cases

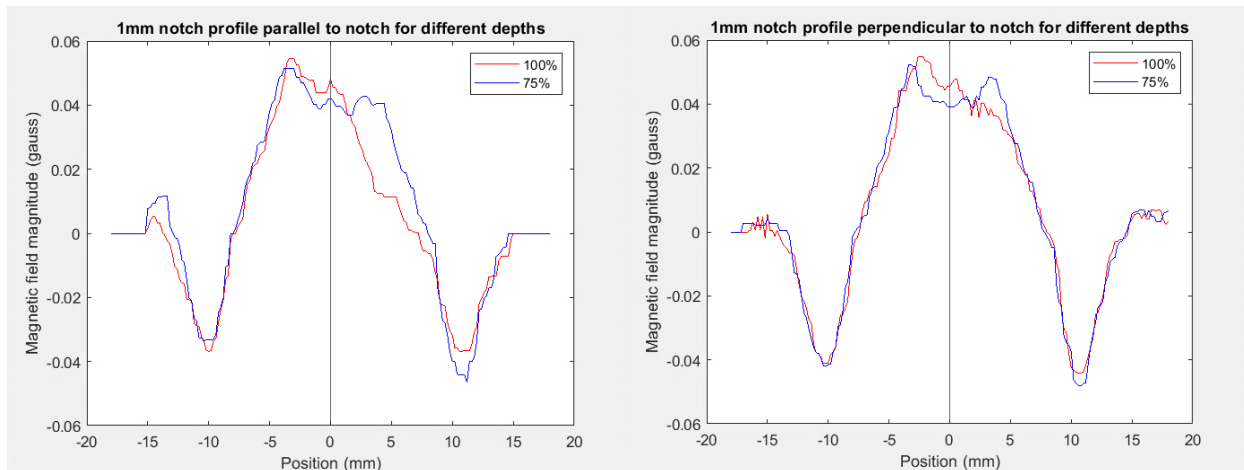


Figure 18: Profiles for the 1 mm notch: parallel (left) and perpendicular (right) to the notch, 100% and 75% notch depth cases

Another qualitative observation for the through-wall penetration notches can be made about the position of the peak value in the parallel-to-notch profiles in Figures 15-18, specifically that the distance of the peak value from the centre of the profile (corresponding to the centre of the fastener hole) is directly proportional to the notch length. The profiles for 1 mm long notches do not display any distinctive features, as for this notch length there is no interaction with the eddy current flow; the notch does not intercept the spiral coil footprint.

The raw peak magnetic field intensity, *i.e.*, before applying any gain to the signal, as a function of the notch length is shown in Figure 19. It is interesting to note that the magnitude of this field is very small and close to the magnetic field of the Earth; however, a component of the field perpendicular to the plate is recorded in this experiment, and is not believed to be affected by the Earth's magnetic field.

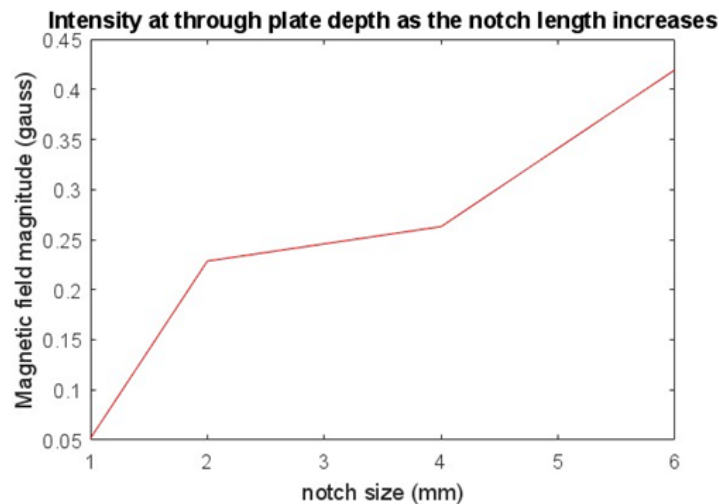


Figure 19: Maximum magnetic field along a profile scan parallel to the through-wall notch

4 Discussion

One of the challenges encountered by the eddy current techniques used for the detection of fatigue cracks initiated at the fastener holes is brought on by the hole itself. It represents a larger and higher volume discontinuity than the crack. In this work we employed a stationary spiral geometry coil, centered around a fastener (and a fastener hole), for inducing eddy currents in the metallic part. The arrangement allowed the eddy currents to flow only in the aluminium plate structure, circumferentially around the fastener hole, while a radial crack interrupts this flow path. In addition to this advantage, a solid-state device, such as the Hall sensor, was used to scan the top surface of the specimen, in a through-transmission arrangement. Due to its high sensitivity to the magnetic field, determined to be 4.5 to 5.0 mV/G, this was expected to also increase the sensitivity to cracks that are not open to the scanning surface. A Hall sensor would directly detect the magnetic field produced by the eddy currents, and not the magnetic flux, as in the case of an inductive probe. The presence of notches of various lengths: 6-, 4-, 2-, and 1-mm, as well as various degrees of penetration from the far side of the plate: 25, 50, 75, and 100% were investigated in this through-transmission eddy current technique. One note needs to be included here about the 1-mm long notch: this notch length was too short to intersect the footprint of the inner turn of the spiral coil, and, therefore, did not produce any meaningful results.

This study demonstrated that there is a direct correlation between the magnetic field signature and the notch length when the notch fully penetrates the thickness of the aluminium plate. However, when the notch was not open to the scanning surface (*i.e.*, top surface of the part), the technique could only detect notches that penetrate 75% through the thickness, as seen in the C-scans of Figure 13. Notches that penetrate only 50% of the part thickness, could not be detected, regardless their respective length. The conductive material above the notch, and directly under the Hall sensor, acts as a shielding layer that does not allow detection of 50% and 25% through-wall notches. The difference in the eddy current flow around a crack grown radially from a fastener hole is shown in Figure 20, with the case of a partially penetrating crack having fewer eddy currents diverted around its tip and closed loops above its geometry.

The C-scans shown in Figure 13 indicate that 75% through wall penetration notches could be detected, as for 6-, 4-, and 2-mm long notches. It is interesting to notice that the sign of the normal-to-surface magnetic field detected by the Hall sensor is the opposite of those of through-thickness notches. This variance could be due to the distribution of the current density and the local magnetic field that was picked up on the top of the conductive test piece. The magnetic field generated by a fully penetrating notch is normal to the part's surface, since the disruption to the eddy current flow is only in the scanning plane. In the

case of partially penetrating notches the eddy current flow is disrupted both in the plane of the aluminium plate and within the thickness; therefore, the normal-to-surface component sensed is much smaller. A schematic representing the eddy current distributions around fully and partially penetrating cracks, grown radially from the fastener hole is shown in Figure 20.

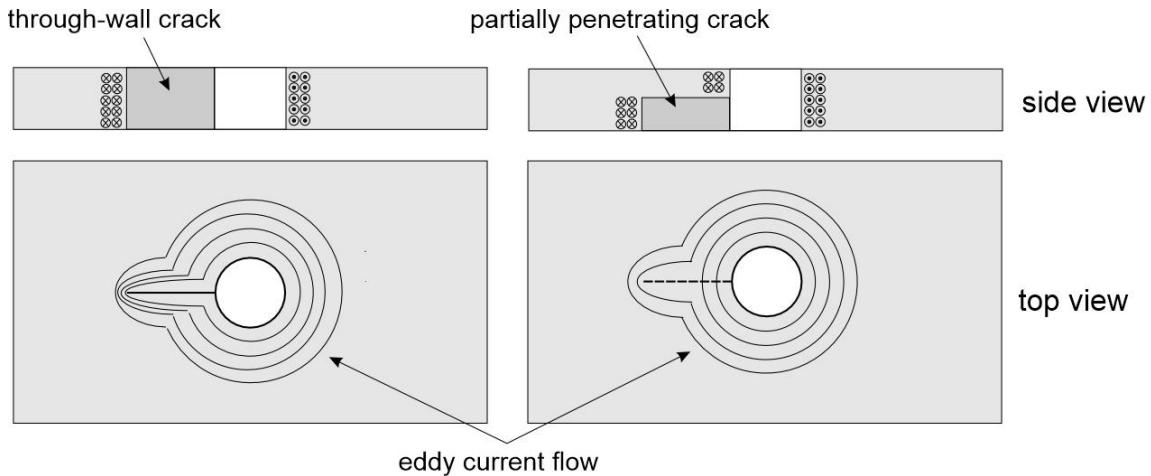


Figure 20: Differences in eddy current flow for a through-wall crack (left) and a partially penetrating one (right)

Possible sources of error in the experiments discussed herein could be variations in centering the driver spiral coil over the hole, imperfect scanning alignment (the scanning axis needed to be parallel to the notch length) and possible lift-off variations from one scan to another. Another potential source of error could be imperfect electrical connections, although efforts were made to keep such errors constant.

5 Conclusion

This report explored the unconventional through-transmission eddy current technique for detecting EDM notches introduced in aluminium plates. The notches were meant to replicate the presence of radial fatigue cracks growing from fastener holes in aircraft structures, due to localized stress concentration. To induce eddy currents, the technique made use of stationary, thin, PCB spiral coils centered on the fastener holes and placed on the back side of the specimen. For detection of the magnetic field created by the eddy currents, the top surface of the aluminium plate was raster-scanned with a Hall-effect sensor. The sensitivity of the Hall sensor was determined experimentally with a Helmholtz coil pair. The technique aimed to detect any non-uniformities in the magnetic field map (*i.e.*, C-scan) produced by EDM notches of various lengths: 6-, 4-, 2-, and 1-mm, as well as various degrees of penetration from the far side of the plate: 25, 50, 75, and 100%.

The experimental results confirm that the notch characteristics, particularly the depth and length, significantly affect the magnetic response as sensed by the Hall device. The field amplitude increased with the notch lengths, as well as with their degree of penetration through the wall of the aluminium plate. A direct correlation between the notch length and the signal strength was established; however, for notches penetrating less than 75% of the wall thickness, no useful signal was detected. This behavior was determined to be due to the shielding effect of the eddy currents flowing in the conductive material on top of the partially penetrating notch.

A future avenue of this work could be the detection of other orthogonal components of the magnetic field, in addition to the normal one used herein. This approach could provide better non-surface crack sensitivity. Other solid-state devices, such as giant magneto-resistive ones or arrays could further improve these investigations.

6 References

1. Ostfeld, A.E.; Deckman, I.; Gaikwad, A.M.; Lochner, C.M.; Arias, A.C. Screen printed passive components for flexible power electronics. *Sci. Rep.* **2015**, *5*, 15959. <https://doi.org/10.1038/srep15959>
2. Hussain, I.; Woo, D.-K. Inductance calculation of single layer planar spiral coil. *Electronics* **2022**, *11*, 750. <https://doi.org/10.3390/electronics11050750>
3. Mandache, C., New trends in eddy current testing, CINDE Journal, Vol. 29, No. 6, **2008**, p. 7-14
4. Honeywell International Inc. (**2024**, October 10). *Linear Hall-effect Sensor ICs: SS490 Series* (Datasheet No. 005843-2, Issue 5). Retrieved from Honeywell Sensing and Internet of Things website: [Linear Hall-effect Sensor ICs: SS490 Series](#)
5. Tatum, J. (2022, March 5). 6.7: Helmholtz coils. In *Electricity and Magnetism* (Tatum). LibreTexts. Retrieved August 28, **2025**, from [6.7: Helmholtz Coils - Physics LibreTexts](#)
6. Eisco labs, Helmholtz coils, <https://www.eiscolabs.com/products/ph0845hel>
7. TecScan. (2023). *TecView™ UT*. Retrieved August 28, **2025**, from TecScan website: <https://tecscan.ca/software/tecview-ut/>
8. The MathWorks, Inc. (n.d.). *MATLAB*. Retrieved August 26, **2025**, from MathWorks website: <https://www.mathworks.com/products/matlab.html>

Appendix A: Surface scans representation

Each C-scan (*i.e.*, surface scan) represents a raster collection of individual data points on each direction: scanning and indexing directions. The data collected using the TecScan instrument and displayed with the TecView software has four components: X, Y, amplitude, and phase. The X and Y components, as shown in Figure A-1, represent the signal in-phase and 90° out-of-phase with the driving waveform, respectively. Their vectorial summation represents the signal amplitude, while the phase representation is the phasor angle at each collected data point.

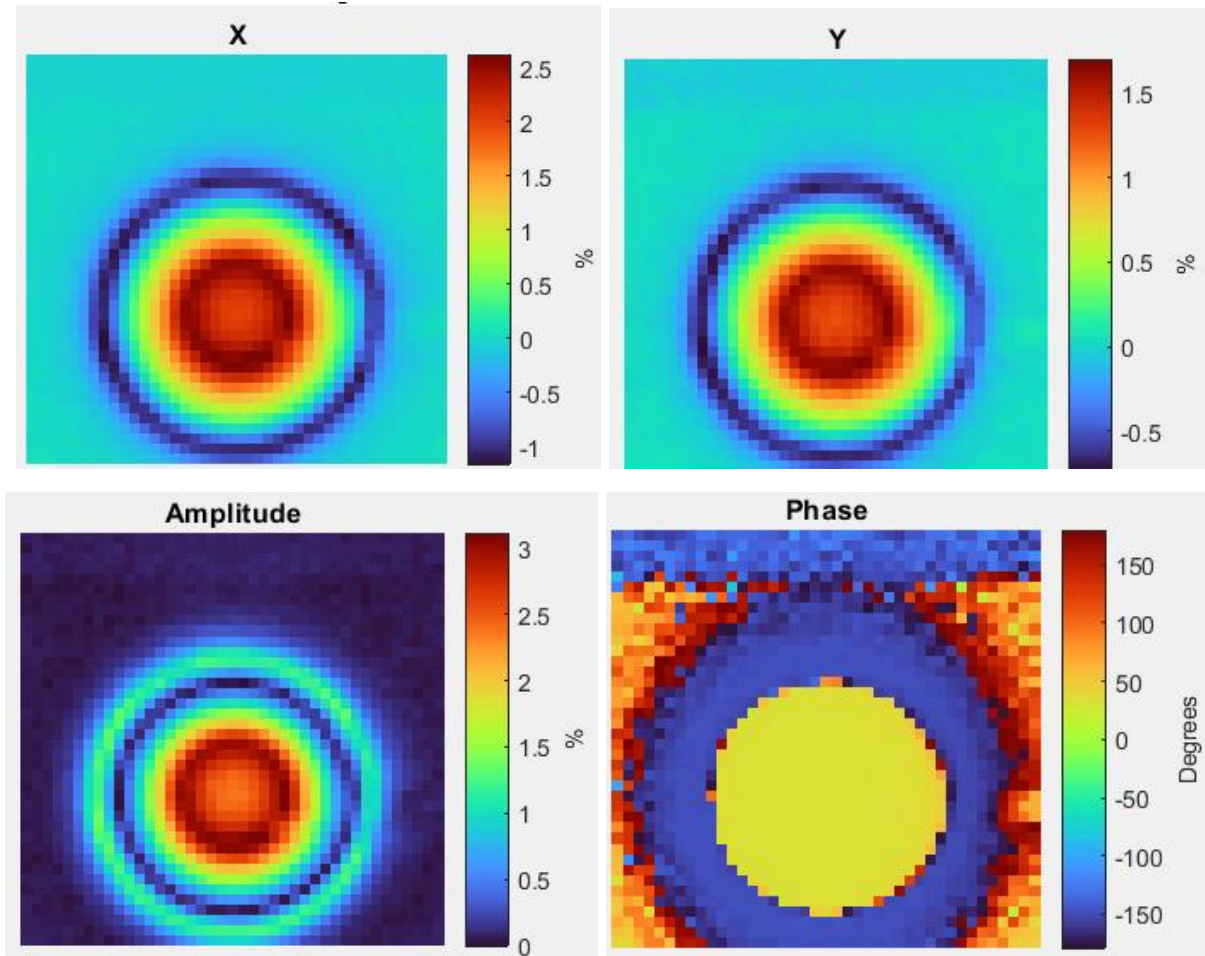


Figure A-1: Result of a scan: X and Y components, as well as amplitude and phase

$$amplitude = \sqrt{X^2 + Y^2} \quad (A-1)$$

$$phase = \arctan \left(\frac{Y}{X} \right) \quad (A-2)$$

Appendix B: MATLAB code examples

B.1 Display C-scan and profile

```

clc, clear
%The purpose of this code is to display the processed C-scan and its corresponding
%profile. The functions used in this sample code are detailed below:

%read raw data file - components X and Y of the C-scan (in this case, for 6 mm notch)
X6mm = readmatrix('Hall sensor coil scans\Trials\trial143\10kHzflexcoilX plate hole
with 6mm notch 0.2mm step 100-75%- correct orientation.csv');
Y6mm = readmatrix('Hall sensor coil scans\Trials\trial143\10kHzflexcoilY plate hole
with 6mm notch 0.2mm step 100-75%- correct orientation.csv');

%sets the desired parameters for the processing. These are the dimensions of the
%padded array, the dimensions of the desired array, and the gain of the instrument.
k=3;
H=250;
W=250;
dist=90;
G=40;

%splits the raw data scans into 2 arrays, one for each hole and notch
[X1006mm, X756mm] = splitting2scans(X6mm);
[Y1006mm, Y756mm] = splitting2scans(Y6mm);

%the phase is rotated and the scan is filtered
[x1006mm, y1006mm, theta1] = phaserotation(X1006mm, Y1006mm, k);
[x756mm, y756mm, theta2] = phaserotation(X756mm, Y756mm, k);

%Function identifies the center of each scan. The tolerance is set to be small but
%acceptable based on the values of the data through trial and error.
level=0.3; tolerance=0.05;
[y1006mmcenterx, y1006mmcentery] = centeridentify(y1006mm, level, tolerance);
[y756mmcenterx, y756mmcentery] = centeridentify(y756mm, level, tolerance);

%the array is padded and shifted based on the center, and then converted from
%percentage to Gauss
[hallpaddedy1006mm]=padshift(y1006mm, y1006mmcenterx, y1006mmcentery, H, W, dist);
[hallpaddedy1006mm]=converttogauss(hallpaddedy1006mm, G);

[hallpaddedy756mm]=padshift(y756mm, y756mmcenterx, y756mmcentery, H, W, dist);
[hallpaddedy756mm]=converttogauss(hallpaddedy756mm, G);

%The parallel profile is identified and selected. The perpendicular profile uses a
%similar process, but across the horizontal line (i,:).
[rows, cols] = size(hallpaddedy1006mm);
vp6=0;
for i=87:92
    vp6=vp6+hallpaddedy1006mm(:,i);
end
vp6 = smoothdata(vp6/6, 'movmedian', 5);
vp675=0;
for i=87:92
    vp675=vp675+hallpaddedy756mm(:,i);

```

```
end
vp675 = smoothdata(vp675/6, 'movmedian', 5);
%figures are displayed and identified
figure(1)
    imshow(hallpaddedy1006mm, colormap=turbo)
    title('6mm notch 100% padded centered')
    clim([min(hallpaddedy1006mm(:)) max(hallpaddedy1006mm(:))])
figure(2)
    imshow(hallpaddedy756mm, colormap=turbo)
    title('6mm notch 75% padded centered')
    clim([min(hallpaddedy756mm(:)) max(hallpaddedy756mm(:))])
figure(3)
    plot(X, vp6, 'r', X, vp675, 'b')
    xline(90*0.2)
    title('6mm notch profile parallel to notch for different depths')
    xlabel('Position (mm)')
    ylabel('Magnetic field magnitude (gauss)')
    legend({'100%', '75%'}, 'location', 'northeast')
```

%FUNCTION splits the 1 scans into 2 arrays with equal dimensions. pads the starting %array by however many squares are needed to make it divisible by 2 so that it can be %split evenly down the middle.

```
function [X100, X75] = splitting2scans(X)
[hx, wx]=size(X);
d=0;

while mod(wx, 2)~=0
    if mod(wx, 2)~=0
        wx=wx+1;
        d=d+1;
        if mod(wx, 2)==0
            A=zeros(hx, wx);
            A(1:end, 1:end-d)=X;
            break
        end
    end
end

dif=wx/2;
if d==0
    X100=X(1:hx, 1:dif);
    X75=X(1:hx, dif:wx);
elseif d~=0
    X100=A(1:hx, 1:dif);
    X75=A(1:hx, dif:wx);
end

end
```

B.2 Apply circular filter and rotation

```
%FUNCTIONS for filtering and rotating functions
```

```
function [X3, Y3, phi] = phaserotation(X1, Y1)
```

```
[X2, Y2] = circularfilter(X1, Y1);
```

```
[X3, Y3, phi] = rotatephase(X2, Y2);
```

```
end
```

```
function [X, Y] = circularfilter(X1, Y1)
```

```
%This function removes the points that are near zero as they are likely to be noise.
```

```
distfromcenter = sqrt((X1).^2 + (Y1).^2);
```

```
r=max(abs(distfromcenter(:)))*0.08;
```

```
%if a point is at a certain distance from 0, it is kept. This distance was determined through trial and error. Anything too close to 0 is removed.
```

```
keep = distfromcenter>r;
```

```
xclean = X1(keep);
```

```
yclean = Y1(keep);
```

```
X=X1.*keep;
```

```
Y=Y1.*keep;
```

```
end
```

```
function [X2, Y2, phi] = rotatephase(X1, Y1)
```

```
%This function performs the lift off compensation and rotates the phase of the data.
```

```
% compute amplitude and phase from X and Y components
```

```
amp = sqrt(X1.^2+Y1.^2);
```

```
phase=atan2(Y1,X1);
```

```
%the phase is shifted so that the amplitude lies mostly along the X axis. This
```

```
%results in small values of Y which make the distortions clearer. (Liftoff
```

```
%compensation)
```

```
for phi = 0:0.01:5
```

```
    phase2=phase-phi;
```

```
    X2= amp.*cos(phase2);
```

```
    Y2= amp.*sin(phase2);
```

```
    if max(max(Y2))<1.4 && min(min(Y2))>-1.45
```

```
        break
```

```
    end
```

```
end
```

```
end
```

B.3 Identify the centre of the fastener hole

```

%FUNCTION used to identify the center of the hole
function [x_center, y_center]=centeridentify(Bgrid, level, tolerance)

%the data is normalised
Bmin = min(Bgrid(:));
Bmax = max(Bgrid(:));
Bnorm = (Bgrid - Bmin) / (Bmax - Bmin);
%all points around a certain value are identified and put into the mask. this value
%is identified through trial and error and approximately lines up one of the rings
%created by the magnetic field
mask = (Bnorm > level - tolerance) & (Bnorm < level + tolerance);

% Extract all point coordinates
[y_all, x_all] = find(mask);

% 1. Estimate rough center by computing multiple diameters and comparing them
x0 = round(mean(x_all));
y0 = round(mean(y_all));
diameter(1)=0;
for i=2:1000
    j=1;
    x1=0;
    y1=0;
    index = find(y_all == y0);
    xi=x_all(index);
    xM = max(xi(:));
    xm = min(xi(:));
    x1 = (xm + xM)/2;
    j=1;

    index2 = find(x_all == x0);

    yi=y_all(index2);

    yM = max(yi(:));
    ym = min(yi(:));
    y1 = (ym + yM)/2;
    x1= round(x1);
    y1= round(y1);
    diameter(i)=yM-ym;
    k=i-1;
    if diameter(i)<=diameter(k)
        break
    end
end

% 2. Compute radius of each point from rough center
radii = sqrt((x_all - x1).^2 + (y_all - y1).^2);

```

```
% 3. Retain only points within 1.5 × median radius (removes far outliers)
r_median = median(radii);
inlier_idx = radii < 1.5 * r_median;

x_pts = x_all(inlier_idx);
y_pts = y_all(inlier_idx);

%Circle Fit by least squares fitting to the points at the level that was selected
%earlier
%  $x^2 + y^2 + Dx + Ey + F = 0$  form (circle)
A = [x_pts, y_pts, ones(size(x_pts))];
Bv = -(x_pts.^2 + y_pts.^2);
coeffs = A \ Bv;

D = coeffs(1);
E = coeffs(2);
F = coeffs(3);
%the centers are found based on the center of the circle that gets fitted
x_center = -D / 2;
y_center = -E / 2;
radius = sqrt((D^2 + E^2)/4 - F);
end
```